Redox Control of the Human Iron-Sulfur Repair Protein MitoNEET Activity via Its Iron-Sulfur Cluster

Marie-Pierre Golinelli-Cohen, Ewen Lescop, Cécile Mons, Sergio Gonçalves, Martin Clémancey, Jerome Santolini, Eric Guittet, Geneviève Blondin, Jean-Marc Latour, Cécile Bouton

THE JOURNAL OF BIOLOGICAL CHEMISTRY VOL. 291, NO. 14, pp. 7583–7593, April 1, 2016

Redox Control of the Human Iron-Sulfur Repair Protein MitoNEET Activity via Its Iron-Sulfur Cluster*

Received for publication, December 21, 2015, and in revised form, February 4, 2016 Published, JBC Papers in Press, February 17, 2016, DOI 10.1074/jbc.M115.711218

Marie-Pierre Golinelli-Cohen[‡1,2], Ewen Lescop[‡1], Cécile Mons[‡3], Sergio Gonçalves[‡], Martin Clémancey[§], Jérôme Santolini[¶], Eric Guittet[‡], Geneviève Blondin[§], Jean-Marc Latour[§], and Cécile Bouton[‡4]

From the [‡]Institut de Chimie des Substances Naturelles (ICSN), CNRS UPR 2301, Université Paris-Sud, Université Paris-Saclay, 91190 Gif-sur-Yvette, France, [§]Université Grenoble Alpes, Laboratoire Chimie et Biologie des Métaux (LCBM), and Commissariat à l'Energie Atomique (CEA), Direction des Sciences du Vivant (DSV), Institut de Recherche en Technologies et Sciences pour le Vivant (iRTSV), LCBM, Equipe Physicochimie des Métaux en Biologie (PMB), and CNRS UMR 5249, LCBM, 38054 Grenoble, France, and [¶]Institute for Integrative Biology of the Cell (I2BC), CEA, CNRS, Université Paris-Sud, Université Paris-Saclay, 91190 Gif-sur-Yvette, France

Human mitoNEET (mNT) is the first identified Fe-S protein of the mammalian outer mitochondrial membrane. Recently, mNT has been implicated in cytosolic Fe-S repair of a key regulator of cellular iron homeostasis. Here, we aimed to decipher the mechanism by which mNT triggers its Fe-S repair capacity. By using tightly controlled reactions combined with complementary spectroscopic approaches, we have determined the differential roles played by both the redox state of the mNT cluster and dioxygen in cluster transfer and protein stability. We unambiguously demonstrated that only the oxidized state of the mNT cluster triggers cluster transfer to a generic acceptor protein and that dioxygen is neither required for the cluster transfer reaction nor does it affect the transfer rate. In the absence of apo-acceptors, a large fraction of the oxidized holo-mNT form is converted back to reduced holo-mNT under low oxygen tension. Reduced holo-mNT, which holds a $[2Fe\text{-}2S]^{+}$ with a global protein fold similar to that of the oxidized form is, by contrast, resistant in losing its cluster or in transferring it. Our findings thus demonstrate that mNT uses an iron-based redox switch mechanism to regulate the transfer of its cluster. The oxidized state is the "active state," which reacts promptly to initiate Fe-S transfer independently of dioxygen, whereas the reduced state is a "dormant form." Finally, we propose that the redox-sensing function of mNT is a key component of the cellular adaptive response to help stress-sensitive Fe-S proteins recover from oxidative injury.

MitoNEET (mNT)[5] is an Fe-S protein of the mammalian outer mitochondrial membrane previously identified as a target of the type II diabetes drug pioglitazone (1). This 13-kDa protein is anchored to the outer mitochondrial membrane by its 32-amino acid N terminus with the major part of the protein, including the C-terminal [2Fe-2S] binding domain, located in the cytosol (2). *In vivo*, the biological activity of mNT has been linked to the regulation of iron/reactive oxygen species homeostasis *in vivo* (3, 4) to cell proliferation in human breast cancer (5) and to the regulation of lipid and glucose metabolism (4).

Crystallographic studies of the soluble form of mNT (mNT_{33-108}) revealed that the protein dimerizes and accommodates one [2Fe-2S] cluster per monomer coordinated by three cysteines (Cys-72, Cys-74, and Cys-83) and one histidine (His-87) in a CDGSH domain (6–9). The cluster is redox-active with a midpoint redox potential of roughly 0 mV at pH 7 (10), and its lability depends on its redox state and on the pH (9, 11). mNT is also able to transfer its cluster *in vitro* to a cyanobacterial (12) and *Escherichia coli* apoferredoxin or to human iron-regulatory protein-1 (IRP-1)/cytosolic aconitase (13). Recently, it has been proposed that mNT plays a specific role in cytosolic Fe-S cluster repair of IRP-1, a key regulator of cellular iron homeostasis in mammalian cells (13).

It has been pointed out previously (12) that oxidation of the mNT cluster is necessary to trigger Fe-S transfer to an apo-recipient. However, it was not possible to identify which parameters, *i.e.* the redox state of the cluster or the presence of dioxygen (O_2), are important for cluster transfer and lability. Furthermore, no biophysical data have been provided on the reduced state of mNT or on protein behavior during the transfer process. In the present study we decided to investigate in depth the respective roles played by the mNT cluster redox state and by dioxygen in these matters. Using a tightly controlled reaction mixture, we unambiguously demonstrated that only the oxidized state of the mNT cluster triggers its transfer to a model receptor protein, without global conformational change of the protein. The transfer process is totally independent of dioxygen and exhibits a conformational switch from a well folded holoprotein to an unfolded apo-form. In contrast, the stability of oxidized holo-mNT is greatly modulated by dioxygen. Finally, we propose that mNT acts as a redox switch

* This work was supported by the Fondation pour la Recherche Médicale (ING20101220983; to S. G.), the Agence Nationale de la Recherche (ANR-13BSV8-0017-01), and the French Infrastructure for Integrated Structural Biology (FRISBI) (ANR-10-INSB-05-01). The authors declare that they have no conflicts of interest with the contents of this article.

[1] Both authors contributed equally to this work.
[2] To whom correspondence may be addressed: Institut de Chimie des Substances Naturelles, UPR 2301-CNRS, 1 avenue de la Terrasse 91190, Gif-sur-Yvette, France. Tel.: 33-1-69-82-30-12; Fax: 33-1-69-07-72-47; E-mail: marie-pierre.golinelli@cnrs.fr.
[3] Recipient of a doctoral grant from the French Ministry of National Education, Research, and Technology.
[4] To whom correspondence may be addressed: Institut de Chimie des Substances Naturelles, UPR 2301-CNRS, 1 avenue de la Terrasse 91190, Gif-sur-Yvette, France. Tel.: 33-1-69-82-30-10; Fax: 33-1-69-07-72-47; E-mail: cecile.bouton@cnrs.fr.

[5] The abbreviations used are: mNT, *Homo sapiens* mitoNEET; FDX, *E. coli* [2Fe-2S] ferredoxin; SOFAST-HMQC, band-selective optimized flip angle short transient heteronuclear multiple-quantum correlation; Bis-Tris, 2-[bis(2-hydroxyethyl)amino]-2-(hydroxymethyl)propane-1,3-diol; IRP-1, human iron-regulatory protein-1.

to transfer its cluster, the reduced state being the dormant physiological state, whereas the oxidized state is active after oxidative insults and reacts promptly to initiate Fe-S transfer.

Experimental Procedures

Expression and Purification of mNT Proteins—Recombinant human mNT_{33-108} and mNT_{44-108} lacking the 32 and the 43 N-terminal amino acids, respectively, were expressed in *E. coli* and purified as described previously (13). Degassed buffers were used during all purification steps. Protein purity was assessed to be >99% using SDS-PAGE and with an optical $A_{280\,nm}/A_{458\,nm}$ ratio near 2.3. The mNT_{44-108} form contains eight additional C-terminal residues derived from the His tag (LEHHHHHH), whereas the mNT_{33-108} form contains, after thrombin cleavage, three additional N-terminal residues derived from the cleavage site (GSH). All the experiments were performed with the mNT_{44-108} form, with the sole exception of the Mössbauer studies performed with the mNT_{33-108} form. For NMR analyses, mNT_{44-108} was expressed on a 1-liter scale in M9 minimal medium (containing 0.001% thiamine-HCl and 10 μM $FeCl_3$), supplemented with 1.0 g of $^{15}NH_4Cl$ and 4.0 g of D-[^{13}C]glucose as the sole nitrogen and carbon sources, respectively. For Mössbauer analyses, mNT_{33-108} was expressed in M9 minimal medium supplemented with ^{57}Fe-enriched ferric chloride.

The *E. coli* apoferredoxin (FDX, full-length construct in pET21b, a gift from Dr. S. Ollagnier de Choudens, Grenoble, France) was expressed and purified as previously described (14).

Protein concentrations were measured using the Bradford assay with bovine serum albumin as standard (15) or absorbance at 280 nm of guanidine-denatured protein using 7115 and 7365 $M^{-1}\cdot cm^{-1}$ (ProtParam) as the extinction coefficient for mNT_{44-108} and FDX, respectively. All protein concentrations were calculated based on monomer equivalents.

Spectroscopic Methods—UV-visible absorption spectra were recorded between 240 and 900 nm with Cary 100 (Agilent) or Safas mc^2 (Monaco) spectrophotometers equipped with a temperature control apparatus set to the desired temperature. For spectra recorded under anaerobic conditions, the cuvette was prepared in a glove box and closed with a septum. Mössbauer spectra of purified ^{57}Fe-labeled mNT_{33-108} were recorded at 4.2 K both in a low field Mössbauer spectrometer equipped with a Janis SVT-400 cryostat and low field permanent magnets and a high field Mössbauer spectrometer equipped with an Oxford Instruments Spectromag 4000 cryostat containing an 8-tesla split-pair superconducting magnet (16). The spectrometer was operated in constant acceleration mode in transmission geometry. The isomer shifts are referenced against that of the room temperature metallic iron foil. Data were analyzed with the program WMOSS (WEB Research, Edina, MN).

For resonance Raman spectroscopy, 50-μl samples of native mNT_{44-108} (200 μM) were prepared in 50 mM phosphate buffer, pH 7.4, and 50 mM NaCl. When required, buffer was made anaerobic by a 2-h flushing with N_2 gas. Anaerobic mNT samples were prepared by performing 20 vacuum/N_2 refilling cycles 4 times every 5 min. The mNT cluster was reduced by adding excess dithionite (5 mM final). Solutions were conditioned in gas-tight quartz EPR tubes and disposed in a homemade spinning cell at room temperature to avoid local heating and to prevent photodissociation and degradation. Raman excitation at 441.6 nm was obtained with a helium-cadmium laser (Kimmon, Tokyo, Japan). Laser power was set at 30 milliwatts. Resonance Raman spectra were recorded using a modified single-stage spectrometer (Jobin-Yvon T64000, HORIBA Jobin Yvon S.A.S., Chilly Mazarin, France) equipped with a liquid N_2-cooled back-thinned CCD detector. Stray scattered light was rejected using a holographic notch filter (Kaiser Optical Systems, Ann Arbor, MI). Slit width was set at 100 μm. Spectra were recorded as the co-addition of 60 individual spectra with CCD exposure times of 60 s each. Four successive sets of such spectra, obtained with two distinct samples, were then averaged. Spectral accuracy was estimated to be $\sim$1 cm^{-1}. Spectral resolution was about 3 cm^{-1}. Baseline correction was performed using GRAMS 32 software (Galactic Industries, Salem, NH).

Nuclear magnetic resonance (NMR) experiments were carried out using a Bruker Avance III 800 MHz spectrometer equipped with a TCI cryoprobe. Two-dimensional ^{1}H,^{15}N SOFAST-HMQC spectra (17) were recorded using a 250 μM His-tagged ^{13}C,^{15}N-labeled holo-mNT_{44-108} protein sample at 298 K in the specified buffers. When experiments were performed under anaerobic conditions, an NMR tube equipped with a valve to maintain anaerobic conditions was used. To extend the backbone assignment from a previous study (18), a set of additional BEST-type triple resonance experiments (19) was carried out, including HNCO, HN(CO)CA, HNCA, HN(CO)CACB, HNCACB, and HN(CA)CO.

In Vitro mNT_{44-108} Cluster Loss and Transfer—Reaction buffers comprised 100 mM NaCl and 50 mM Bis-Tris pH 6.2 and were prepared under the conditions specified under "Results." Reactions were followed by UV-visible absorption or NMR spectroscopies, or by migration of aliquots taken at specific times on a 16% native PAGE gel run under aerobic conditions and stained with colloidal Coomassie Blue.

For the cluster transfer reaction, apo-FDX was prepared by heat cluster disassembly at 90 °C of purified holo-FDX in the presence of 10 mM DTT and 10 mM EDTA followed by purification on a NAP-5 column (GE Healthcare) equilibrated with 50 mM Tris-HCl, pH 7.0, and 100 mM NaCl. Apo-FDX was preincubated with 5 mM DTT for 30 min at room temperature under anaerobic conditions to ensure cysteine reduction. When specified, DTT was removed, and buffer was exchanged with 50 mM Bis-Tris, pH 6.2, 100 mM NaCl using a Micro Bio-Spin Size Exclusion column (Bio-Rad).

UV-Visible Absorption Spectroscopy for Cluster Transfer/Loss Kinetics—The 240–900-nm absorption spectra of the reaction were recorded over time and corrected for baseline variations at 900 nm. We paid particular attention to changes in absorbance at 458 nm and 415 nm, which are characteristic of the [2Fe-2S] cluster bound to mNT and FDX, respectively. At time t, the extent of the cluster transfer was determined using the ratio $R(t) = A_{415}/A_{458}$, whereas the extent of loss of the mNT cluster was determined using $R(t) = A_{458}$. Reaction progress at time t was estimated as $(R(t) - R_{initial})/(R_{final} - R_{initial})$,

with $R_{initial}$, the initial R value at time 0, and R_{final}, the R value at the time necessary for reaction completion.

Iron Quantification—Free and total iron was quantified using a bathophenanthroline colorimetric assay (20). For total iron quantification of a 100-μl sample, 10 μl of perchloric acid 54%, 72 μl of bathophenanthroline 1.7 mg/ml, 18 μl of sodium ascorbate 76 mg/ml, 10 μl of saturated ammonium acetate solution, and 140 μl of water were added. After 15 min at room temperature, the absorbance at 535 nm was measured. Free iron quantification was performed on a 250-μl sample using the same protocol except that perchloric acid and water were not added.

Results

Role of Dioxygen in the Transfer of the mNT Fe-S to Apoferredoxin—In previous studies, a role for mNT in Fe-S transfer/repair to apo-acceptors has been proposed (12, 13). However, a clear distinction could not be drawn between the specific role of dioxygen in the cluster transfer reaction and the role played by the redox state of the mNT Fe-S cluster, because these studies were performed under aerobic conditions with the oxidized form of mNT and under anaerobic conditions with the reduced form. To address this issue, we first compared, under aerobiosis and anaerobiosis, the ability of oxidized holo-mNT to transfer its cluster to *E. coli* [2Fe-2S] FDX, a protein widely used as a model recipient protein (21–23). To set up the cluster transfer reaction, apo-FDX was reduced by DTT, and the reductant was removed. Then, thiol-reduced apo-FDX was mixed with oxidized holo-mNT under either aerobic or anaerobic conditions, and Fe-S transfer was followed using UV-visible absorption (Fig. 1*A*). As apo-FDX does not absorb in the 300–650-nm wavelength range, the initial spectra in Fig. 1*A* (*black curves*) of both mixtures were characteristic of the oxidized holo-mNT, with absorption peaks at 338, 458, and 542 nm (9). The characteristic 415-nm band of oxidized holo-FDX (see UV-visible absorption spectrum of oxidized holo-FDX in Fig. 1*B*) progressively increased over time in aerobiosis and anaerobiosis and reached a plateau after ~3 h. Analysis of the reaction end products on a native gel confirmed the switch from the holo- to apo-form of mNT and vice versa for FDX regardless of the aerobic and anaerobic conditions (Fig. 1*C*). This first set of experiments clearly demonstrates that dioxygen is not necessary for the cluster transfer mechanism.

In a second step, the effect of dioxygen on the rate of cluster transfer was carefully determined by examining the change over time of the ratio of the absorbances at 415 and 458 nm, which reflects the transfer reaction progress, under aerobiosis and anaerobiosis. As shown in Fig. 1*D*, *left panel*, dioxygen *per se* did not affect the rate of Fe-S transfer by mNT ($t_{½}$ = 25 ± 6 min for both conditions).

In parallel, the effect of dioxygen on the $[2Fe\text{-}2S]^{2+}$ cluster lability of mNT was investigated. We prepared a solution of holo-mNT and followed the change in absorbance at 458 nm over time. Only roughly 10% of the proteins underwent cluster loss after 900 min under anaerobic conditions (Fig. 1*D*, *right panel*, *squares*). By contrast, the rate of cluster loss was increased ~20-fold in the presence of dioxygen (Fig. 1*D*, *right panel*, *circles*), with a $t_{½}$ of 360 ± 50 min under aerobic conditions. Altogether, these data unambiguously demonstrate that

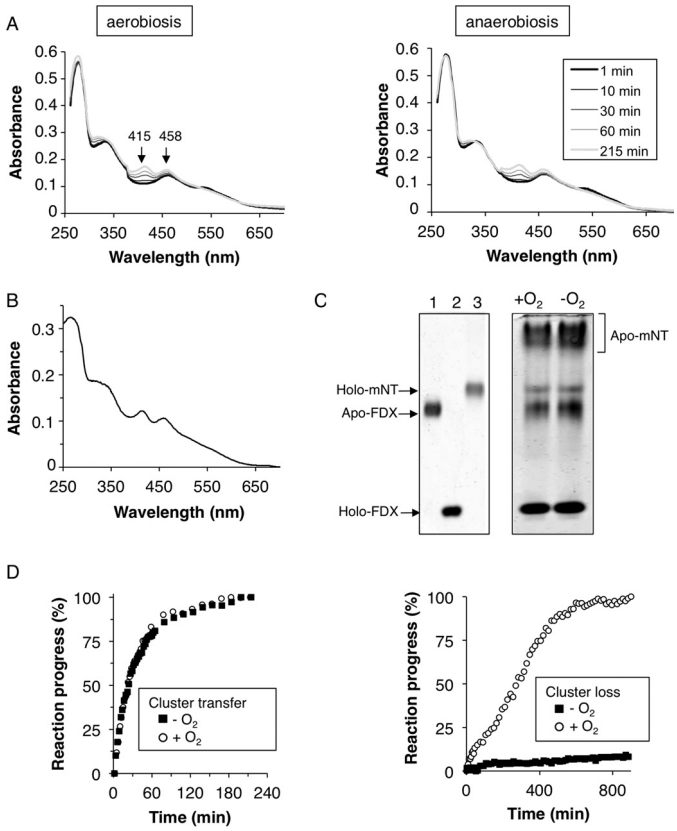

FIGURE 1. **Dioxygen does not affect cluster transfer, whereas it increases cluster lability.** Reactions were performed in 50 mM Bis-Tris, pH 6.2, 100 mM NaCl at 25 °C using oxidized holo-mNT and apo-FDX (20 μM concentrations of each protein) for cluster transfer reactions and 20 μM oxidized holo-mNT for cluster disassembly reactions. Each experiment was performed at least three times; one representative experiment is presented. Reactions were followed by UV-visible absorption spectroscopy (*A* and *D*) or migration on a 16% non-reducing native gel (*C*). For cluster transfer reactions, DTT used for apo-FDX reduction was removed before transfer. Reactions were performed either under aerobic conditions (*A*, *left panel*; *C*, $+O_2$ *lane*; *D*, *circles*) or under anaerobic conditions (*A*, *right panel*; *B*, $-O_2$ *lane*; *D*, *squares*). *A*, change in the UV-visible absorption spectrum over time of the cluster transfer reactions performed under aerobic (*left*) or anaerobic (*right*) conditions. *B*, UV-visible absorption spectrum of oxidized *E. coli* holo-ferredoxin. *C*, after 16 h of reaction, products were analyzed on a 16% non-reducing native gel with 30 μM apo-FDX (*lane 1*), holo-FDX (*lane 2*), and holo-mNT (*lane 3*) as migration controls. For the reaction presented, mNT was roughly 95% in the apo-form when approximately 60% of the apo-FDX was converted in the holo-form. *D*, change in reaction progress over time for the transfer reactions presented in *panel A* (*left panel*) and for cluster disassembly reactions (*right panel*) under anaerobic (*filled squares*) and aerobic (*empty circles*) conditions.

although cluster instability of oxidized holo-mNT is strongly increased by dioxygen, the latter did not bear on the initiation and/or the rate of the mNT cluster transfer reaction.

Role of the Redox State of the mNT Cluster in the Fe-S Transfer Reaction—Once the role of dioxygen in the Fe-S transfer reaction was ruled out (Fig. 1), we decided to focus on how mNT cluster redox state triggers Fe-S transfer using UV-visible absorption spectroscopy. We first took advantage of the limited reducing capacity of DTT at pH below 7 (24) and checked that the addition of DTT at pH 6.2 to the oxidized holo-mNT did not affect the spectrum (Fig. 2*A*, *gray dotted curve versus gray curve*). In contrast, the addition of DTT at pH 8.0 profoundly modified the spectrum (*black dotted curve*), which was characteristic of the reduced holo-mNT form (Fig. 2*A*, *black curve*) (9). In a second step we used this pH-dependent reducing prop-

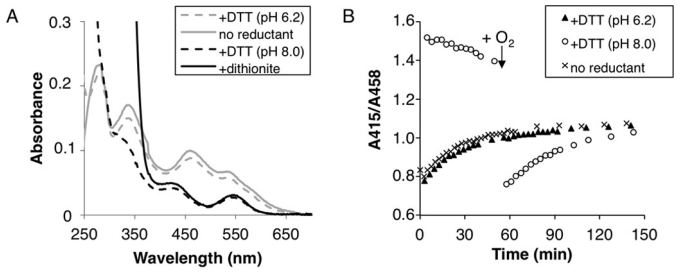

FIGURE 2. **Oxidation of the mNT cluster triggers cluster transfer.** *A*, characterization by UV-visible absorption spectroscopy of holo-mNT treated with reductant in different conditions. Spectra of 20 μM mNT were recorded after 10 min under anaerobic conditions in 50 mM Bis-Tris, pH 6.2, 100 mM NaCl in the absence of reductant (*gray line*) with 2 mM dithionite (*black line*) or with 5 mM DTT at pH 6.2 (*dotted gray line*) or in 50 mM Tris-HCl, pH 8.0, 100 mM NaCl at pH 8.0 (*dotted black line*). *B*, holo-mNT was used without pretreatment (*crosses*) or pretreated with 5 mM DTT at pH 6.2 (*triangles*) or at pH 8.0 (*circles*). Then transfer reactions were performed at pH 6.2 under anaerobic conditions (*crosses* and *triangles*) or under anaerobic conditions up to 50 min and then under aerobic conditions (*circles*). Transfer reactions were followed by plotting the ratio of the absorbances at 415- and 458 nm over time. Results for one representative experiment are presented.

erty of DTT to carefully examine the influence of mNT cluster redox state on the cluster transfer reaction. Two Fe-S transfer experiments were performed in parallel under anaerobiosis (Fig. 2*B*). The reaction mixtures were identical in composition (*e.g.* holo-mNT, apo-FDX, and DTT in buffer at pH 6.2) except that they differed in the redox state of the holo-mNT. In mixture 1, DTT was added to mNT diluted in the transfer buffer at pH 6.2 (no reduction), whereas in mixture 2, DTT was added to mNT at pH 8.0 before dilution in the transfer buffer at pH 6.2 (reduction). We showed that Fe-S transfer occurred only in mixture 1 and that the progress of the reaction was identical to that of the control reaction without DTT (Fig. 2*B*, compare *triangles* and *crosses*). In mixture 2, in which holo-mNT was reduced by DTT, the A_{415}/A_{458} ratio decreased slightly under anaerobiosis, reflecting a very limited reoxidation of the mNT cluster. After exposure to air at 50 min, the A_{415}/A_{458} ratio rapidly dropped in response to Fe-S cluster reoxidation, and the Fe-S transfer was then possible (Fig. 2*B*, *circles*). Altogether, these data unambiguously demonstrate the key role of the $[2Fe\text{-}2S]^{2+}$ state of the mNT cluster as a crucial signal in allowing Fe-S transfer to be processed.

Spectroscopic Characterization of Reduced Holo-mNT—The oxidized form of holo-mNT, which mediates Fe-S transfer, has been well characterized *in vitro* (13, 18, 25). However, reduced holo-mNT, which is inactive as an Fe-S transfer protein, is poorly characterized. We, therefore, combined resonance Raman, Mössbauer, and NMR spectroscopies in an attempt to distinguish the [2Fe-2S] cluster structure/environment and backbone conformational changes of holo-mNT upon reversible redox switch. Fig. 3*A* shows the Fe-S stretching region of the resonance Raman spectra of both oxidized (*black curve*) and dithionite-reduced holo-mNT (*red curve*). In aerobic conditions, major vibrational bands of the mNT spectrum were observed at 269, 284, 330, 350, 393, and 412 cm^{-1}, which is characteristic of the oxidized $[2Fe\text{-}2S]^{2+}$ cluster containing mNT (25). Upon the addition of excess dithionite under anaerobic conditions, these markers nearly completely disappeared, whereas a strong band at 321 cm^{-1} appeared with

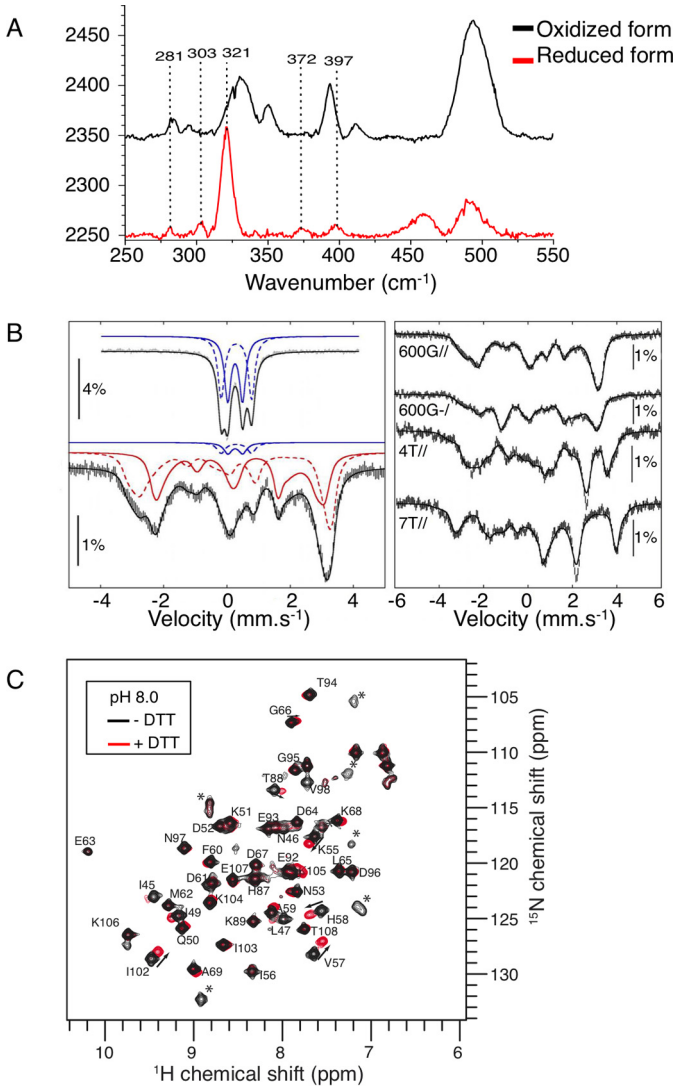

FIGURE 3. **Characterization of *Homo sapiens* oxidized and reduced holoforms of mNT.** *A*, resonance Raman characterization of oxidized (*black*) and reduced (*red*) mNT. The 250–550 cm^{-1} spectral region of the low frequency resonance Raman spectra was analyzed with a laser excitation at 441.6 nm. *Dashed lines* highlight the vibrational band contributions of the reduced cluster. *B*, characterization by Mössbauer spectroscopy of dithionite (10 mM)-reduced mNT (1 mM) in 200 mM sodium phosphate, pH 8.0, 50 mM NaCl, recorded at 4.2 K in a magnetic field of 600 G applied parallel to the direction of the γ-rays (*bottom*, *left*) and spectra recorded at 4.2 K in magnetic fields of 600 G applied parallel and perpendicular, and 4 and 7 tesla (*T*) applied parallel to the direction of the γ-rays (*right*). The *solid* and *dashed blue lines* represent the contributions of $[2Fe\text{-}2S]^{2+}$ clusters, and the *solid* and *dashed red lines* represent the contributions of $[2Fe\text{-}2S]^{+}$ clusters. The *solid black lines* are theoretical simulations with parameters mentioned in Table 1. The spectrum of oxidized mNT at 4.2 K in a magnetic field of 600 G applied parallel to the direction of the γ-rays is given (*top left*) for comparison. *C*, characterization by NMR. ^{15}N SOFAST-HMQC spectra were collected for a 250 μM ^{15}N-labeled mNT sample in 50 mM Tris-HCl, pH 8.0, 100 mM NaCl under anaerobic conditions with (*red*) or without (*black*) 10 mM DTT at 800 MHz and 298 K. The $^{1}H,^{15}N$ cross-peaks are labeled according to their amino acid number. Cross-peaks indicated by a *star* are not assigned. The largest chemical shift perturbations upon addition of DTT are indicated by *arrows*.

additional bands at 281, 303, 372, and 397 cm^{-1}. The intense band at 321 cm^{-1} might correspond to the Fe^{III}-S^{t} stretching mode that has been reported at 319, 325, or 328 cm^{-1} for the reduced $[2Fe\text{-}2S]^{+}$ clusters in putidaredoxin and ferredoxins from *Spinacia oleracea* and *Clostridium pasteurianum*, respectively (26, 27).

TABLE 1
Mössbauer parameters of selected [2Fe-2S]$^{+}$ proteins
Pp, P. putida; Ae, A. aeolicus; Ec, E. coli; Hs, Homo sapiens.

	Ae FdI[a]		*Hs* mNT[b]		*Ec* IscR[c]		*Pp* Rieske[d]	
Parameters	Fe^{III}	Fe^{II}	Fe^{III}	Fe^{II}	Fe^{III}	Fe^{II}	Fe^{III}	Fe^{II}
δ (mm/s)	0.30	0.62	0.32	0.68	0.33	0.70	0.30	0.75
ΔE_Q (mm/s)	1.0	3.0	1.07	3.15	1.09	3.4	0.65	−3.2
η	0	0.0	0	0.4	0.5	0.48	0	−2
A_x (MHz)	−56	11	−55.7	29.5	−34.9	20.9	−55	13
A_y (MHz)	−49	27	−46.7	28.5	−38.8	21.9	−48	14
A_z (MHz)	−42	33	−41.6	9.1	−32.3	6.5	−44	30

[a] From Ref. 29.
[b] This work.
[c] From Ref. 30.
[d] From Ref. 31.

In parallel, dithionite reduction of oxidized holo-mNT also causes drastic changes in the Mössbauer spectra. Fig. 3*B* presents the low-field Mössbauer spectrum of reduced ^{57}Fe-labeled mNT (*left bottom*) that now extends from −3.7 to +4 mm/s and, for comparison, that of the oxidized [2Fe-2S]$^{2+}$ form (*left top*) (13). The spectrum of the reduced holo-mNT is similar to those of the [2Fe-2S]$^{+}$ forms of *Pseudomonas putida* putidaredoxin (28), *Aquifex aeolicus* ferredoxin I (29) (both protein clusters are coordinated by four cysteines), *E. coli* IscR (30) (three cysteines and one histidine), and *P. putida* Rieske protein (31) (two histidines and two cysteines). Because the [2Fe-2S]$^{+}$ center of these reduced proteins has an S = 1/2 ground state resulting from the antiferromagnetic coupling of high spin Fe^{3+} (S = 5/2) and Fe^{2+} (S = 2) cations, field-dependent experiments were performed up to 7 tesla (Fig. 3*B*, *right*) and confirmed this ground state. Then, a set of four spectra was analyzed with the spin Hamiltonian of an S = 1/2 ground state. The inclusion of a small amount (6%) of unreduced mNT [2Fe-2S]$^{2+}$ cluster (*blue trace* in Fig. 3*B*, *left bottom*) was necessary to fit the spectrum correctly. The Mössbauer parameters of the [2Fe-2S]$^{+}$ mNT cluster are listed in Table 1 together with those of [2Fe-2S]$^{+}$ proteins. Their comparison highlights the close similarity of mNT with IscR, an iron and oxidative stress [2Fe-2S] sensor (32, 33), in agreement with their common Cys_3-His environment.

Finally, ^{15}N-labeled mNT was analyzed by NMR spectroscopy after reduction with DTT. As shown in Fig. 3*C*, the folded ^{15}N-labeled [2Fe-2S]$^{2+}$ mNT (*black spectrum*) exhibits a well dispersed ^{15}N SOFAST-HMQC spectrum (17) at pH 8, and >90% of the peaks were assigned based on a previous study (18) and additional triple resonance experiments. Seven unassigned cross-peaks that are visible in the two-dimensional spectrum (labeled with a *star* in Fig. 3*C*) could be tentatively assigned to residues in the Val-70–Gly-85 fragment that lie in the vicinity of the Fe-S cluster. The peak broadening in triple resonance experiments, which hampered assignment of these residues, most likely results from the paramagnetic enhanced relaxation induced by the Fe-S cluster. Upon the addition of DTT, the two-dimensional spectrum showed small but significant modifications (Fig. 3*C*, *red spectrum*). The largest effects were observed for the unassigned cross-peaks, which could not be followed upon the addition of DTT without additional experiments because they underwent either large shifts or severe line broadening. For assigned cross-peaks, peak shifts were moderate, thus facilitating their assignment. The largest shifts for assigned residues were observed for residues located in the second shell centered on the cluster, including Ile-45, Leu-47, Ile-49, Asn-53, Lys-55, and Val-57 in the N-terminal loop L1, His-58 and Ile-102 in the β-sheet, and Thr-88 in the helix α1. In contrast, no significant shift was observed for residues away from the cluster. We then removed DTT from the solution and observed that the two-dimensional NMR spectrum recorded under anaerobic conditions remained identical to the red spectrum (Fig. 3*C*) for at least 24 h (data not shown). Finally, exposing the solution to air resulted in rapid recovery in the original spectrum, which corresponds to the [2Fe-2S]$^{2+}$-mNT (*black spectrum*). On the basis of these experiments, we concluded that the peak shifts observed upon DTT addition are related to the Fe-S redox state and not to DTT binding and that the reduced mNT state is relatively stable. The significant peak shifts in the vicinity of the Fe-S cluster upon reduction may reveal a change in Fe-S cluster paramagnetic properties or a local conformational change in this region. The amino acid residues that do not experience chemical shift variations upon protein reduction are localized away from the Fe-S cluster, and many belong to the β-sheet that stabilizes the dimeric mNT structure. This NMR study, therefore, demonstrates that the tertiary and quaternary structure of mNT is globally conserved upon reduction.

Transfer of the mNT Cluster Induces the Unfolding of the Protein—As depicted in Fig. 4*A*, we next investigated the NMR spectroscopic behavior of a mixture containing both reduced holo-mNT and apo-FDX by switching from aerobic conditions and pH 8.0 (*Step 1*) to anaerobic acidic conditions (*Step 2*) and then to oxidized cluster by exposure to air (*Step 3*). When ^{15}N-labeled holo-mNT was incubated under aerobic conditions with apo-FDX in a 1:1 ratio in the presence of DTT at pH 8.0, no chemical shift variations were observed in the ^{15}N SOFAST-HMQC spectra (data not shown) as compared with that recorded in the absence of apo-FDX (Fig. 3*C*, *red spectrum*). In both experiments mNT was reduced. This suggests that intermolecular interactions between reduced holo-mNT and apo-FDX, if there are any, are very weak (K_d larger than ~1 mM). In a second step (Step 2), we switched the mixture to an acidic environment (pH 6.0) under anaerobic conditions, and DTT was removed. The HMQC spectrum of the solution revealed that after buffer exchange, mNT was essentially in its reduced holo-form (Fig. 4*B*, *Spectrum 1*, *circles*) with a minor amount (<10%) of the apo-form (Fig. 4*B*, *Spectrum 1*, *triangles*). Twenty-six hours later, the spectrum (*Spectrum 2*) had not changed, indicating great stability of the reduced holo-mNT without cluster loss or transfer to apo-FDX despite the slightly acidic environment and the presence of the apo-acceptor (*Spectrum 2*, Fig. 4*B*). The reaction mixture was then exposed to air by opening the NMR tube, and a series of HMQC spectra were collected over 20 h. We observed that the peaks characteristic of the reduced holo-form at time 0 (Fig. 4*B*, *spectrum 3*, *circles*) completely disappeared at the end of the reaction (*Spectrum 4*), whereas the intensity of the peaks corresponding to the apo-form (*triangles*) (13, 18) strongly increased. Peaks originating from the oxidized holo-mNT are visible in the spectra at the end of the reaction (*squares*), albeit at very low intensity. The final state of mNT is largely unfolded as judged from the narrow

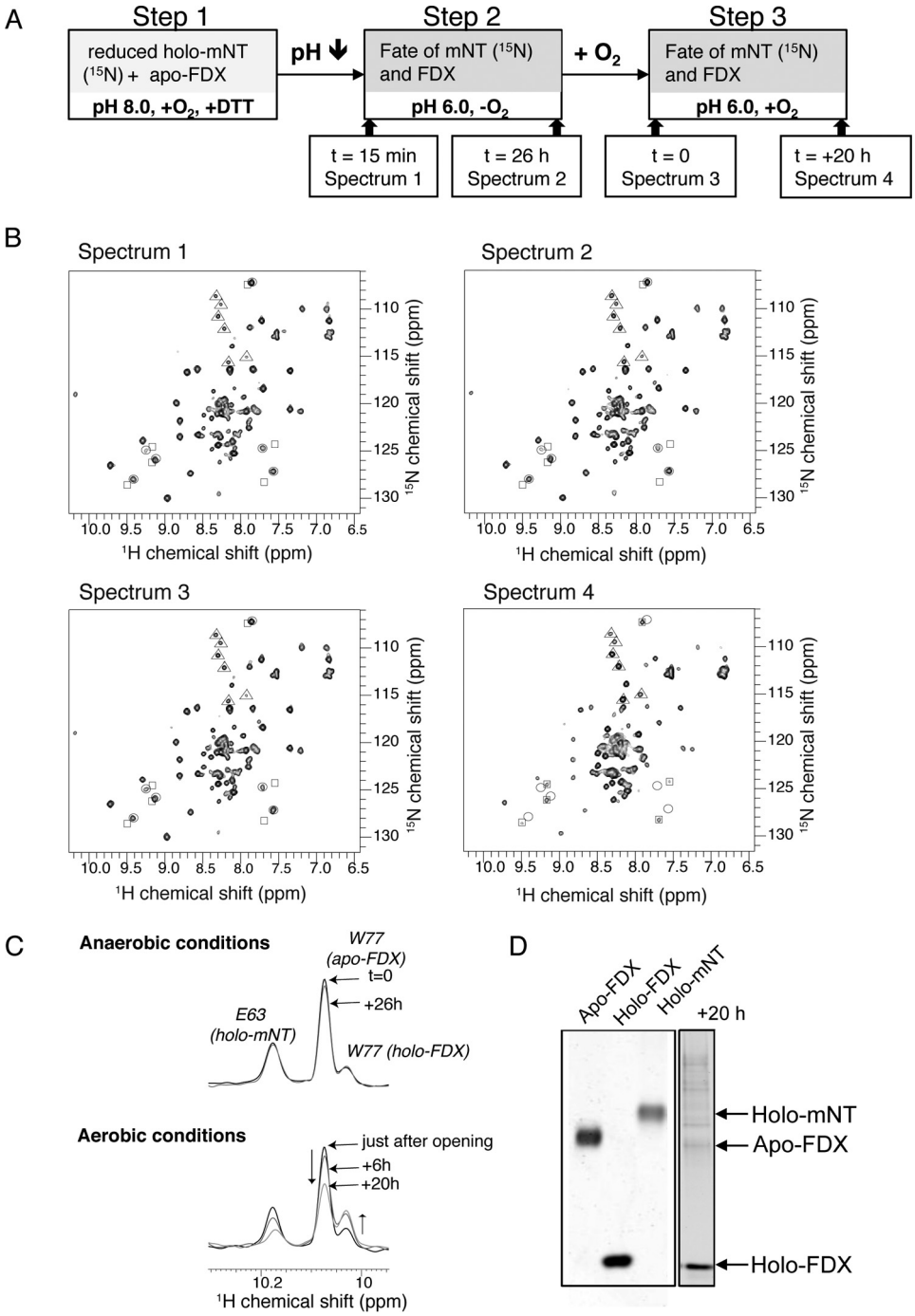

FIGURE 4. **Spectroscopic behavior of both reduced and oxidized mNT in Fe-S transfer.** *A*, schematic representation of the protocol for the Fe-S cluster transfer reaction followed by NMR. *Step 1*, a mixture of 250 μM ^{15}N-labeled mNT and 250 μM unlabeled FDX was prepared in 50 mM Tris-HCl, pH 8.0, 100 mM NaCl, 10 mM DTT under aerobic conditions. *Step 2*, the reaction mixture was then exchanged for reaction buffer at pH 6.0 (50 mM Bis-Tris, pH 6.0, 100 mM NaCl) in a glove box and finally stored in an NMR tube under anaerobic conditions. ^{15}N SOFAST-HMQC spectra were collected at 298 K and 800 MHz 15 min (*Spectrum 1*) and 26 h (*Spectrum 2*) after sample preparation. *Step 3*, at time 26 h the NMR tube valve was opened (aerobic conditions), and two additional NMR ^{15}N SOFAST-HMQC were collected immediately (*Spectrum 3*) and 20 h (*Spectrum 4*) after the opening of the NMR tube. *B*, ^{15}N SOFAST-HMQC spectra were collected at 298 K and 800 MHz as described in *panel A*. Peaks characteristic of the reduced and oxidized holo-mNT are indicated by *circles* and *squares*, respectively, whereas peaks characteristic of the apo-mNT are indicated by *triangles*. *C*, close-up view in the 9.9–10.3 ppm region of one-dimensional ^{15}N-decoupled ^{1}H spectra collected during the course of the experiment at times t = 0 (*black*) and 26 h (*gray*) under anaerobic conditions and just after tube opening (*black*) followed by spectra collected 6 h (*dark gray*) and 20 h (*gray*) after tube opening. The peaks characteristic of the backbone amide proton of holo-mNT Glu-63 and Trp-77 side chain HN in apo- and holo-FDX are labeled. Under aerobic conditions, changes in their amplitude over time are highlighted by *arrows*. *D*, 20 h after NMR tube opening, reaction products were analyzed on a 16% reducing native gel.

^{1}H NMR spectral dispersion for the dominant species in solution.

Additional one-dimensional ^{15}N-decoupled ^{1}H spectra were also collected during this experiment to follow apo-FDX during the cluster transfer reaction. *Panel C* of Fig. 4 represents a close-up view centered at 10.08 ppm on the signal assigned to the NH side chain proton of the single tryptophan 77 in apo-FDX. This ^{1}H spectrum remained unchanged throughout the

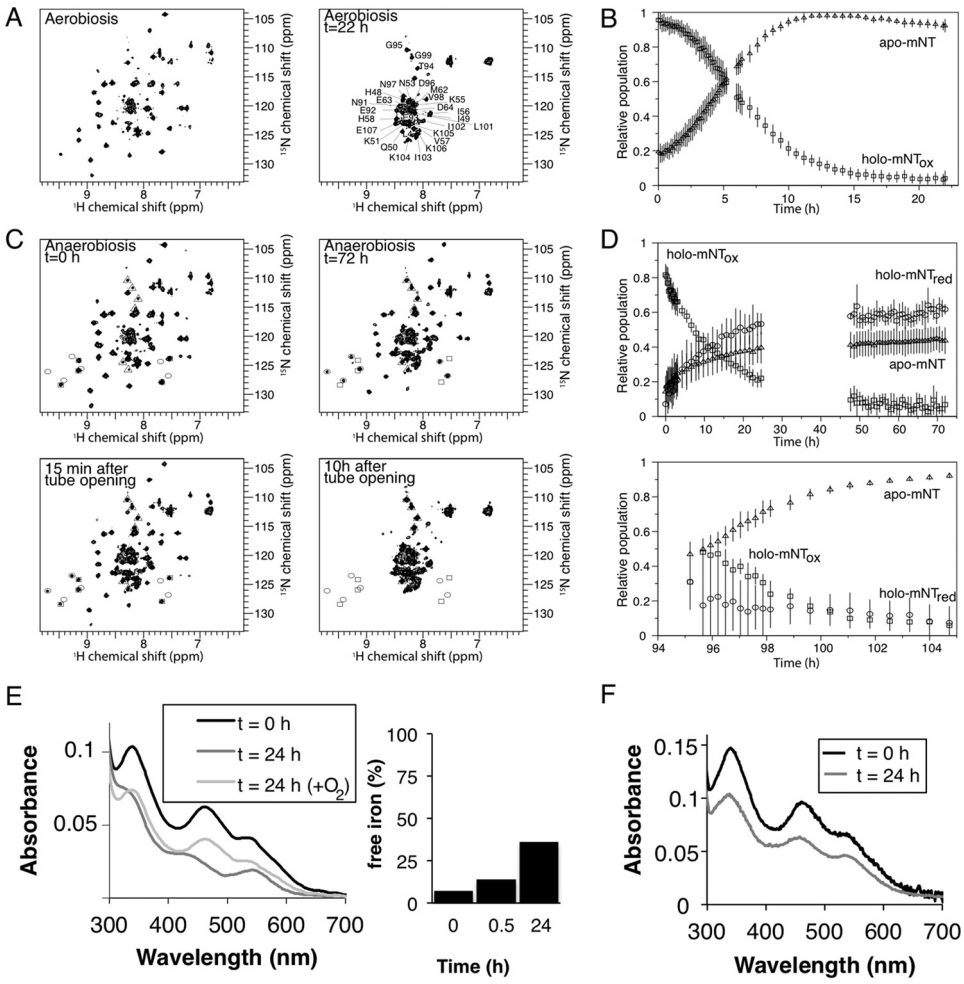

FIGURE 5. **Denaturation of oxidized holo-mNT under anaerobic conditions results in reduction of the remaining holo-mNT.** Studies were performed with 250 μM ^{15}N-labeled mNT in 50 mM Bis-Tris, pH 6.2, 100 mM NaCl at 298 K. *A*, mNT denaturation under aerobic conditions followed by NMR spectroscopy. ^{15}N SOFAST-HMQC spectra were collected at 298 K and 800 MHz just after buffer exchange to pH 6.2 (*left*) and 22 h later (*right*). *B*, the averages of the normalized amplitude of peaks characteristic of oxidized holo-mNT (*square*) and apo-mNT (*triangle*) were plotted over time. *C*, mNT denaturation under anaerobic conditions followed by NMR spectroscopy. ^{15}N SOFAST-HMQC spectra were collected at 298 K and 800 MHz at the beginning of the reaction (*C*, *top left*), after 72 h (*C*, *top right*), just after NMR tube opening (*C*, *bottom left*), and 10 h after tube opening (*C*, *bottom right*). Peaks characteristic of the reduced and oxidized holo-mNT are indicated by *circles* and *squares*, respectively, whereas peaks characteristic of the apo-mNT are indicated by *triangles*. *D*, the averaged normalized peak amplitude of oxidized (*square*) and reduced (*circle*) holo-mNT and apo-mNT (*triangle*) was plotted for the anaerobic (*upper panel*) and aerobic (*lower panel*) periods. *E*, mNT denaturation followed by UV-visible absorption spectroscopy under anaerobic conditions. *Left panel*, spectra were recorded at the beginning of the reaction (*black curve*, *left panel*), after 24 h under anaerobic conditions (*dark gray curve*) and just after cuvette opening (*gray curve*). The experiment was performed at least three times; one representative experiment is presented (*right panel*). For the experiment presented in the *left panel*, free iron concentration was measured at different times as described under "Experimental Procedures" and expressed as a percentage of total iron (*right panel*). *F*, the same experiment as in *E* was performed in the presence of 200 μM potassium cyanide.

time course under anaerobic conditions, which confirmed that the system reached a stable situation with reduced holo-mNT and apo-FDX intact. However, after opening the NMR tube, the peak associated with the apo-FDX tryptophan group decreased in intensity, and concomitantly, a new peak appeared in its vicinity that was assigned to the same proton in holo-FDX (Fig. 4*C*, *lower panel*). The final products were also run on a 16% native gel, and the results show that the band corresponding to holo-FDX was present (Fig. 4*D*). Our findings clearly demonstrate the unfolding of the mNT protein backbone concomitantly with the transfer of its cluster to apo-FDX. These data also confirm the great structural stability of the reduced holo-mNT even in a slightly acidic environment and the initiation of cluster transfer by oxidation of the mNT cluster.

Denaturation Process of Oxidized Holo-mNT—To gain further insight into the strong differential stability of the oxidized holo-mNT in the presence or absence of dioxygen as observed in Fig. 1*D*, we performed an in-depth NMR spectroscopy investigation of the mechanism of denaturation of oxidized holo-mNT under aerobic and anaerobic conditions at pH 6.2. Under aerobic conditions (Fig. 5, *A* and *B*), the well dispersed two-dimensional SOFAST-HMQC spectrum of oxidized holo-mNT was replaced over time by a much less dispersed spectrum characteristic of apo-mNT (Fig. 5*A*), in agreement with the loss of cluster and of protein fold (13, 18). We integrated signal intensities to calculate the normalized amplitudes for the holo- and apo-forms (Fig. 5*B*), which demonstrated that all oxidized holo-mNT was converted into apo-mNT after ~15 h. We further analyzed the apo-mNT form and assigned the observable resonances to their corresponding amino acids (Fig. 5*A*, *right panel*). We could unambiguously assign the Met-44–Asn-53 and Asn-91–Glu-107 fragments, but the Pro-54–His-90 frag-

ment remained unassigned because signal intensity was too low in the two-dimensional and three-dimensional spectra. The chemical shift values of assigned fragments were then analyzed using the δ2D algorithm (34), which provides the propensity for each amino acid to adopt secondary structures (α-helix, β-strand, random coil, or polyproline II). In the apo-form, the δ2D analysis (data not shown) revealed that assigned amino acids essentially populated the random coil structures (propensity >80%), whereas the α, β, and polyproline II secondary structure elements were not significantly populated (propensity <10–15%). This suggests the absence of significant residual secondary structure elements in the assigned region and demonstrates the high flexibility of apo-mNT at the N-terminal (Met-44–Asn-53) and C-terminal (Asn-91–Glu-107) extremities. In contrast, the core of the protein sequence corresponding to the Pro-54–His-90 fragment gave rise to weak intensities, which may reveal for this region a more complex behavior, such as aggregation or conformational transitions occurring at the chemical shift (millisecond) timescale, in agreement with previous observations (11).

Under anaerobic conditions, the denaturation process contrasts with that in aerobiosis (Fig. 5, *C* and *D*). At the beginning of the reaction, the spectrum was characteristic of the oxidized holo-form of mNT (Fig. 5*C*, $t = 0$ h, *squares*). After 72 h, the peaks of the oxidized holo-form completely disappeared and were replaced by those of the reduced holo-form (*circles*) and of the apo-form (*triangles*). At intermediate times (5–20 h, see Fig. 5*D*), the signals corresponding to the three species coexisted in the spectra, which revealed in particular the slow electron exchange between the $[2Fe\text{-}2S]^{2+}$ and $[2Fe\text{-}2S]^{+}$ clusters. To facilitate the analysis, amplitudes of the peaks characteristic of the three species were quantified, normalized, and averaged (Fig. 5*D*) and were used as reporters of the time-dependent population for the three species. This quantification indicated that, under anaerobic conditions, a stable state was reached after 50 h with 40% of apo-mNT and 60% of reduced holo-mNT. In contrast to the cluster loss under aerobic conditions that appears to be non-exponential (Fig. 5*B*), the disappearance of oxidized holo-mNT and the formation of reduced holo-mNT and of apo-mNT follow exponential curves under anaerobiosis (Fig. 5*D*). Then, upon NMR tube opening, the amplitude of the peaks for the reduced state dropped rapidly (within 30 min), whereas those for the oxidized holo-form concomitantly reached ~50% that of their initial amplitude (Fig. 5, *panel C*, *15 min after tube opening*, and *D*), in agreement with the rapid reoxidation of the protein in the presence of dioxygen. Ten hours after tube opening, the spectrum (Fig. 5*C*, *10 h after tube opening*) was virtually identical to that obtained in *panel* $t = 22h$ of Fig. 5*A* and characteristic of the apo-form of mNT, in agreement with the cluster loss of oxidized holo-mNT at this pH under aerobic conditions.

In parallel, a similar experiment was performed using UV-visible absorption (Fig. 5*E*, *left panel*). After 24 h under anaerobic conditions, the remaining proportion of mNT clusters was reduced (*dark gray curve*). After cuvette opening (*gray curve*), re-oxidation of the cluster occurred rapidly, and the amplitude of the visible part of the spectrum was ~40% lower than in the initial spectrum. This result was confirmed by free iron quantification, which showed that just after cuvette opening roughly 40% of the iron was free (Fig. 5*E*, *right panel*, *24 h bar*). This set of experiments thus firmly demonstrated that cluster loss of the oxidized holo-mNT under anaerobic conditions results in the formation of ~40% apo-mNT and 60% reduced holo-mNT. It also confirmed the results obtained by NMR experiments (Fig. 5*C*) regarding the very high stability of the reduced cluster at slightly acidic pH (pH 6.2). Finally, we checked whether the inorganic sulfur released by cluster disassembly explains the reduction of the remaining protein-bound cluster. The same UV-visible experiment was thus performed in the presence of potassium cyanide, which has the ability to trap free sulfur by formation of a thiocyanate (35) (Fig. 5*F*). After 24 h under anaerobic conditions, the amplitude of the UV-visible absorption spectrum, still characteristic of the oxidized form, was as high as 70% of the initial spectrum. Therefore, we concluded that the inorganic sulfur released by cluster disassembly is capable of reducing *in vitro* the remaining protein-bound cluster as illustrated in Fig. 6.

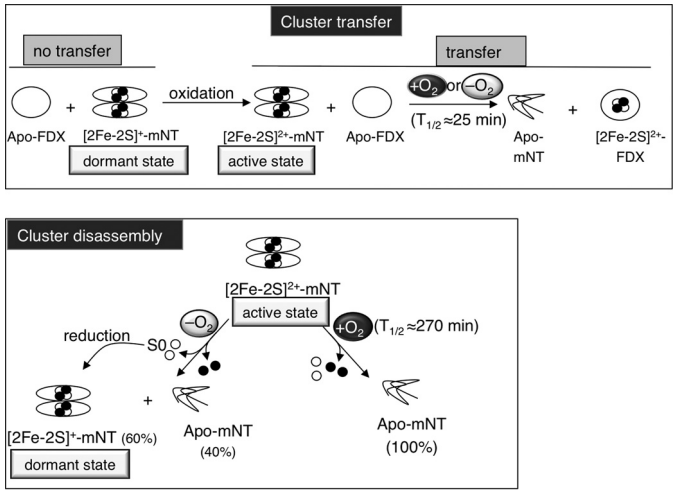

FIGURE 6. **Scheme summarizing the data obtained on both Fe-S transfer and disassembly of mNT.** *Upper panel*, at a slightly acidic pH reduced holo-mNT is a very stable well folded $[2Fe\text{-}2S]^{+}$ protein unable to transfer its Fe-S to an apo-acceptor. Under oxidizing conditions, the $[2Fe\text{-}2S]^{+}$ is converted to $[2Fe\text{-}2S]^{2+}$ without major global conformational change of the protein. This regulatory redox switch is sufficient to trigger Fe-S transfer from mNT to apo-FDX. This cluster transfer occurs without protein-protein interaction visible by NMR and is independent of the presence of dioxygen. *Lower panel*, in contrast, in the absence of an apo-acceptor, dioxygen increases cluster instability and speeds up cluster disassembly of the oxidized holo-mNT. Finally, incubation of oxidized holo-mNT under anaerobic conditions leads to the formation of unfolded apo-mNT and reduced holo-mNT due to reduction of the remaining holo-protein by the released inorganic sulfur.

Discussion

The main purpose of the present study was to uncover the mechanism by which mNT repairs damaged Fe-S proteins. To this end, NMR and UV-visible absorption spectroscopies were predominantly used to follow the cluster transfer process. Our findings demonstrate that the redox state of the mNT cluster, and not dioxygen, is a critical signal that triggers mNT cluster transfer to an apo-recipient. Initiation of the transfer operates once the inactive reduced holo-mNT is converted to the active oxidized holo-mNT form, intriguingly without global conformational change.

Recently, it has been proposed that the reduced holo-form of mNT is present in quiescent mammalian cells (36). Here, we provide evidence that the reduced form of holo-mNT is an extremely stable $[2Fe\text{-}2S]^{+}$ form with a global fold similar to that of the oxidized $[2Fe\text{-}2S]^{2+}$ form. This form, hereafter referred to as dormant form, is strongly resistant to cluster loss by disassembly or by transfer to a recipient protein, even at a slightly acidic pH, which enables the oxidized holo-mNT to release its cluster (9). Remarkably, acidic pH has been measured in the inner membrane space of mitochondria, in the vicinity of the endogenous mNT environment (37). Therefore, the high stability of reduced holo-mNT deserves to be highlighted. It has been reported that reduction of the mNT cluster is coupled with two protonations referred to as proton-coupled electron transfer (10) as in the case of the Rieske protein, another [2Fe-2S] protein involving histidine coordination of its cluster (two cysteines and two histidines). As with mNT, no major conformational change was induced by reduction of the Rieske cluster (38), and only the residues in the vicinity of the cluster might be affected (39). In the case of mNT, the reduction of the cluster is coupled to two protonations of the ϵ-nitrogen of the histidine ligand and of another unknown residue (11). Noticeably, the cluster binding module of mNT is more compact than usual in Fe-S proteins (7). Both ligand and non-ligand residues (Tyr-71, Ser-77, Pro-81, Phe-82, Asp-84) are involved in a complex hydrogen bond network (6, 8), which critically stabilizes the cluster (7). It is, therefore, tempting to suggest that the high stability of holo-mNT upon reduction is a direct consequence of the modification of the hydrogen bond network.

In two recent studies it has been proposed that mNT is an Fe-S transfer/repair enzyme, playing a role under conditions of oxidative stress (12, 13). Here, we showed that the process of cluster transfer is initiated only by changing the redox state of the mNT cluster from the reduced $[2Fe\text{-}2S]^{+}$ to the oxidized $[2Fe\text{-}2S]^{2+}$ form. In addition, triggering this process intriguingly occurs without major change on the global tertiary or quaternary conformation of mNT. It is worth recalling that (i) the cluster of the oxidized form of holo-mNT is less stable when the pH becomes more acidic under aerobic conditions (11), and (ii) changes in intracellular pH regulate a number of normal and pathological processes, and dramatic differences in cell behavior can be triggered by small modifications of local pH (40). Such subtle changes in acidic pH can occur in living cells after oxidative insults (41, 42). Therefore, we may envision that lowering the intracellular pH during oxidative stress is a regulatory process that cooperates with that of the redox switch of the mNT cluster to facilitate Fe-S transfer initiation by mNT. During the transfer reaction, we further show that oxidized holo-mNT is almost fully converted into an unfolded apo-form *in vitro*. Importantly, this latter form can be refolded back into the oxidized holo-form through re-insertion of its Fe-S cluster (11, 13). Taking these findings into consideration, it is tempting to suggest that mNT may pursue several rounds of Fe-S transfer *in vitro* once its cluster has been re-inserted. Moving forward, the mitochondrial ISC assembly and export machineries, which continuously supply unfolded apo-mNT with its clusters in living cells (13), may contribute to several cycles of Fe-S transfer through every molecule of mNT to repair damaged Fe-S proteins.

Whereas the mechanism of the mNT transfer reaction is starting to be investigated, no data are available on the termination of the transfer reaction. This final step might be driven by the glutathione reductase, which is able to reduce oxidized holo-mNT *in vitro* (43). Nevertheless, by investigating oxidized holo-mNT stability under anaerobic conditions, we observed that disassembly of its cluster drives the reduction of the remaining holo-protein, making the reduced holo-mNT the major form. The inorganic sulfur released during disassembly may explain the reduction as observed for spinach ferredoxin (35) and the fumarate nitrate reductase (44). From these observations, we propose that the released inorganic sulfur may undergo oxidation to S0, leading to reduction of the remaining holo-mNT. Furthermore, reduction of the oxidized holo-mNT in the absence of apo-acceptors, under the physiological low dioxygen tension found in numerous human tissues, may have important physiological meanings, especially regarding termination of the mNT transfer reaction. In living cells, once Fe-S proteins have been repaired by mNT and oxidative stress is controlled, we consider that oxidized holo-mNT may exert auto-feedback control by stopping the repair of Fe-S-client proteins through its own conversion back into its dormant reduced holo-form.

The present study clearly shows that mNT acts as a redox sensor to perform its transfer function. Interestingly, as regard other known cluster transfer proteins, including A-type proteins, SufB, IscU, and GRX, the transfer reactions were typically performed under anaerobic conditions (45). To our knowledge the respective roles of dioxygen and of the redox state of the cluster in the reaction have never been studied. Looking ahead, a challenging issue would be to search for some other cluster transfer proteins functioning as a redox switch. Interestingly, more and more Fe-S proteins are being found to use the redox state of their cluster to regulate their activity. AirSR (anaerobic iron-sulfur cluster-containing redox sensor regulator or YhcSR) is a two-component signal transduction system that regulates *Staphylococcus aureus* virulence (46). AirS is a [2Fe-2S] kinase that modulates the AirR transcription regulator and is active only when its cluster is oxidized (47). Under conditions of oxidative stress, SoxR triggers the activation of the transcription of the soxS genes by oxidation of its cluster (48), without major structural changes (49). The bacterial DinG helicase is active only when its H_2O_2-resistant cluster is oxidized (50). In the case of the base excision repair enzymes, it was shown that oxidized MutY has a greater affinity for DNA and that DNA-bound MutY can be reduced by another distally bound MutY through DNA-mediated charge transfer (51). Thus, all known Fe-S proteins that control their activity through the redox state of the Fe-S cluster are involved in the cellular response after an oxidative stress. Moreover, all of them function in the same way: the inactive form is the reduced state, whereas they all become active by oxidation of their cluster. In this regard, the mitochondrial respiratory chain is a major source of superoxide and the resulting product from its dismutation, H_2O_2 (52). Another source of mitochondrial H_2O_2 is the $p66^{shc}$ adaptor protein that oxidizes cytochrome *c* and is involved in aging

dysfunction (53). Mitochondrial production of reactive oxygen species, notably H_2O_2, is involved in redox signaling (54), whereas excess production of mitochondrial oxidants has been associated with a variety of diseases (55). We, therefore, propose that when there are abnormalities in mitochondrial respiration, which occur in metabolic and stress diseases, activation of mNT by increased reactive oxygen species production (36) constitutes a compensatory mechanism by which cells repair damaged cytosolic client Fe-S proteins like the iron master regulator IRP-1 (13). This regulation may constitute an adaptive mechanism that avoids imbalance of cellular iron metabolism, which is prone to generate an iron-dependent Fenton reaction in mitochondria. By limiting the action of IRP-1 in fueling iron to mitochondria (56, 57), mNT would protect the cell against ferroptosis, a unique iron- and ROS-dependent form of non-apoptotic cell death (58).

Author Contributions—M.-P. G.-C., E. L., and C. B. designed the study. M.-P. G.-C., C. M., and S. G. performed protein purifications and biochemical assays. E. L. and E. G. conducted the NMR studies, J. S. conducted the resonance Raman study, and M. C., G. B., and J.-M. L. conducted the Mössbauer study. M.-P. G.-C., E. L., and C. B. wrote the manuscript. All authors approved the final version of the manuscript .

Acknowledgments—We thank Dr. Eric Jacquet (Institut de Chimie des Substances Naturelles, ICSN) for allowing use of the Akta purifier (GE Healthcare), Dr. Nelly Morellet for help with NMR, and Dr. Jean-Marc Moulis for fruitful discussions. We are grateful to Dr. Jean-Claude Drapier (ICSN) for all the fruitful discussions and for critical reading of the manuscript. This work has benefited from the facilities and expertise of the TEFOR Molecular Biology Unit, I2BC, Gif Research Center.

References

1. Colca, J. R., McDonald, W. G., Waldon, D. J., Leone, J. W., Lull, J. M., Bannow, C. A., Lund, E. T., and Mathews, W. R. (2004) Identification of a novel mitochondrial protein ("mitoNEET") cross-linked specifically by a thiazolidinedione photoprobe. *Am. J. Physiol. Endocrinol. Metab.* **286,** E252–E260
2. Wiley, S. E., Murphy, A. N., Ross, S. A., van der Geer, P., and Dixon, J. E. (2007) MitoNEET is an iron-containing outer mitochondrial membrane protein that regulates oxidative capacity. *Proc. Natl. Acad. Sci. U.S.A.* **104,** 5318–5323
3. Nechushtai, R., Conlan, A. R., Harir, Y., Song, L., Yogev, O., Eisenberg-Domovich, Y., Livnah, O., Michaeli, D., Rosen, R., Ma, V., Luo, Y., Zuris, J. A., Paddock, M. L., Cabantchik, Z. I., Jennings, P. A., and Mittler, R. (2012) Characterization of Arabidopsis NEET reveals an ancient role for NEET proteins in iron metabolism. *Plant Cell* **24,** 2139–2154
4. Kusminski, C. M., Holland, W. L., Sun, K., Park, J., Spurgin, S. B., Lin, Y., Askew, G. R., Simcox, J. A., McClain, D. A., Li, C., and Scherer, P. E. (2012) MitoNEET-driven alterations in adipocyte mitochondrial activity reveal a crucial adaptive process that preserves insulin sensitivity in obesity. *Nat. Med.* **18,** 1539–1549
5. Sohn, Y. S., Tamir, S., Song, L., Michaeli, D., Matouk, I., Conlan, A. R., Harir, Y., Holt, S. H., Shulaev, V., Paddock, M. L., Hochberg, A., Cabanchick, I. Z., Onuchic, J. N., Jennings, P. A., Nechushtai, R., and Mittler, R. (2013) NAF-1 and mitoNEET are central to human breast cancer proliferation by maintaining mitochondrial homeostasis and promoting tumor growth. *Proc. Natl. Acad. Sci. U.S.A.* **110,** 14676–14681
6. Hou, X., Liu, R., Ross, S., Smart, E. J., Zhu, H., and Gong, W. (2007) Crystallographic studies of human MitoNEET. *J. Biol. Chem.* **282,** 33242–33246
7. Lin, J., Zhou, T., Ye, K., and Wang, J. (2007) Crystal structure of human mitoNEET reveals distinct groups of iron sulfur proteins. *Proc. Natl. Acad. Sci. U.S.A.* **104,** 14640–14645
8. Paddock, M. L., Wiley, S. E., Axelrod, H. L., Cohen, A. E., Roy, M., Abresch, E. C., Capraro, D., Murphy, A. N., Nechushtai, R., Dixon, J. E., and Jennings, P. A. (2007) MitoNEET is a uniquely folded 2Fe-2S outer mitochondrial membrane protein stabilized by pioglitazone. *Proc. Natl. Acad. Sci. U.S.A.* **104,** 14342–14347
9. Wiley, S. E., Paddock, M. L., Abresch, E. C., Gross, L., van der Geer, P., Nechushtai, R., Murphy, A. N., Jennings, P. A., and Dixon, J. E. (2007) The outer mitochondrial membrane protein mitoNEET contains a novel redox-active 2Fe-2S cluster. *J. Biol. Chem.* **282,** 23745–23749
10. Bak, D. W., Zuris, J. A., Paddock, M. L., Jennings, P. A., and Elliott, S. J. (2009) Redox characterization of the FeS protein MitoNEET and impact of thiazolidinedione drug binding. *Biochemistry* **48,** 10193–10195
11. Bak, D. W., and Elliott, S. J. (2013) Conserved hydrogen bonding networks of MitoNEET tune Fe-S cluster binding and structural stability. *Biochemistry* **52,** 4687–4696
12. Zuris, J. A., Harir, Y., Conlan, A. R., Shvartsman, M., Michaeli, D., Tamir, S., Paddock, M. L., Onuchic, J. N., Mittler, R., Cabantchik, Z. I., Jennings, P. A., and Nechushtai, R. (2011) Facile transfer of [2Fe-2S] clusters from the diabetes drug target mitoNEET to an apo-acceptor protein. *Proc. Natl. Acad. Sci. U.S.A.* **108,** 13047–13052
13. Ferecatu I., Gonçalves S., Golinelli-Cohen M. P., Clémancey M., Martelli A., Riquier S., Guittet E., Latour J. M., Puccio H., Drapier J. C., Lescop E., and Bouton C. (2014) The drug diabetes MitoNEET governs a novel trafficking pathway to rebuild an Fe-S cluster into cytosolic aconitase/Iron Regulatory Protein 1. *J. Biol. Chem.* **289,** 28070–28086
14. Ta, D. T., and Vickery, L. E. (1992) Cloning, sequencing, and overexpression of a [2Fe-2S] ferredoxin gene from *Escherichia coli*. *J. Biol. Chem.* **267,** 11120–11125
15. Bradford, M. M. (1976) A rapid and sensitive method for the quantitation of microgram quantities of protein utilizing the principle of protein-dye binding. *Anal. Biochem.* **72,** 248–254
16. Carboni, M., Clémancey, M., Molton, F., Pécaut, J., Lebrun, C., Dubois, L., Blondin, G., and Latour, J. M. (2012) Biologically relevant heterodinuclear iron-manganese complexes. *Inorg. Chem.* **51,** 10447–10460
17. Schanda, P., Kupce, E., and Brutscher, B. (2005) SOFAST-HMQC experiments for recording two-dimensional heteronuclear correlation spectra of proteins within a few seconds. *J. Biomol. NMR* **33,** 199–211
18. Zhou, T., Lin, J., Feng, Y., and Wang, J. (2010) Binding of reduced nicotinamide adenine dinucleotide phosphate destabilizes the iron-sulfur clusters of human mitoNEET. *Biochemistry* **49,** 9604–9612
19. Lescop, E., Schanda, P., and Brutscher, B. (2007) A set of BEST triple-resonance experiments for time-optimized protein resonance assignment. *J. Magn. Reson.* **187,** 163–169
20. Moulis, J. M., and Meyer, J. (1982) Characterization of the selenium-substituted 2 [4Fe-4Se] ferredoxin from *Clostridium pasteurianum*. *Biochemistry* **21,** 4762–4771
21. Bonomi, F., Iametti, S., Ta, D., and Vickery, L. E. (2005) Multiple turnover transfer of [2Fe2S] clusters by the iron-sulfur cluster assembly scaffold proteins IscU and IscA. *J. Biol. Chem.* **280,** 29513–29518
22. Chahal, H. K., and Outten, F. W. (2012) Separate FeS scaffold and carrier functions for $SufB_2C_2$ and SufA during *in vitro* maturation of [2Fe2S] Fdx. *J. Inorg. Biochem.* **116,** 126–134
23. Gupta, V., Sendra, M., Naik, S. G., Chahal, H. K., Huynh, B. H., Outten, F. W., Fontecave, M., and Ollagnier de Choudens, S. (2009) Native *Escherichia coli* SufA, coexpressed with SufBCDSE, purifies as a [2Fe-2S] protein and acts as an Fe-S transporter to Fe-S target enzymes. *J. Am. Chem. Soc.* **131,** 6149–6153
24. Cleland, W. W. (1964) Dithiothreitol, a new protective reagent for Sh groups. *Biochemistry* **3,** 480–482
25. Tirrell, T. F., Paddock, M. L., Conlan, A. R., Smoll, E. J., Jr., Nechushtai, R., Jennings, P. A., and Kim, J. E. (2009) Resonance Raman studies of the (His)(Cys)3 2Fe-2S cluster of MitoNEET: comparison to the (Cys)4 mutant and implications of the effects of pH on the labile metal center. *Biochemistry* **48,** 4747–4752

26. Fu, W., Drozdzewski, P. M., Davies, M. D., Sligar, S. G., and Johnson, M. K. (1992) Resonance Raman and magnetic circular dichroism studies of reduced [2Fe-2S] proteins. *J. Biol. Chem.* **267,** 15502–15510
27. Xiao, Y., Tan, M. L., Ichiye, T., Wang, H., Guo, Y., Smith, M. C., Meyer, J., Sturhahn, W., Alp, E. E., Zhao, J., Yoda, Y., and Cramer, S. P. (2008) Dynamics of *Rhodobacter capsulatus* [2Fe-2S] ferredoxin VI and *Aquifex aeolicus* ferredoxin 5 via nuclear resonance vibrational spectroscopy (NRVS) and resonance Raman spectroscopy. *Biochemistry* **47,** 6612–6627
28. Münck, E., Debrunner, P. G., Tsibris, J. C., and Gunsalus, I. C. (1972) Mössbauer parameters of putidaredoxin and its selenium analog. *Biochemistry* **11,** 855–863
29. Meyer, J., Clay, M. D., Johnson, M. K., Stubna, A., Münck, E., Higgins, C., and Wittung-Stafshede, P. (2002) A hyperthermophilic plant-type [2Fe-2S] ferredoxin from *Aquifex aeolicus* is stabilized by a disulfide bond. *Biochemistry* **41,** 3096–3108
30. Fleischhacker, A. S., Stubna, A., Hsueh, K. L., Guo, Y., Teter, S. J., Rose, J. C., Brunold, T. C., Markley, J. L., Münck, E., and Kiley, P. J. (2012) Characterization of the [2Fe-2S] cluster of *Escherichia coli* transcription factor IscR. *Biochemistry* **51,** 4453–4462
31. Wolfe, M. D., Altier, D. J., Stubna, A., Popescu, C. V., Münck, E., and Lipscomb, J. D. (2002) Benzoate 1,2-dioxygenase from *Pseudomonas putida*: single turnover kinetics and regulation of a two-component Rieske dioxygenase. *Biochemistry* **41,** 9611–9626
32. Giel, J. L., Nesbit, A. D., Mettert, E. L., Fleischhacker, A. S., Wanta, B. T., and Kiley, P. J. (2013) Regulation of iron-sulphur cluster homeostasis through transcriptional control of the Isc pathway by [2Fe-2S]-IscR in *Escherichia coli*. *Mol. Microbiol.* **87,** 478–492
33. Wu, Y., and Outten, F. W. (2009) IscR controls iron-dependent biofilm formation in *Escherichia coli* by regulating type I fimbria expression. *J. Bacteriol.* **191,** 1248–1257
34. Camilloni, C., De Simone, A., Vranken, W. F., and Vendruscolo, M. (2012) Determination of secondary structure populations in disordered states of proteins using nuclear magnetic resonance chemical shifts. *Biochemistry* **51,** 2224–2231
35. Petering, D., Fee, J. A., and Palmer, G. (1971) The oxygen sensitivity of spinach ferredoxin and other iron-sulfur proteins: the formation of protein-bound sulfur-zero. *J. Biol. Chem.* **246,** 643–653
36. Landry, A. P., and Ding, H. (2014) Redox control of human mitochondrial outer membrane protein MitoNEET [2Fe-2S] clusters by biological thiols and hydrogen peroxide. *J. Biol. Chem.* **289,** 4307–4315
37. Porcelli, A. M., Ghelli, A., Zanna, C., Pinton, P., Rizzuto, R., and Rugolo, M. (2005) pH difference across the outer mitochondrial membrane measured with a green fluorescent protein mutant. *Biochem. Biophys. Res. Commun.* **326,** 799–804
38. Hsueh, K. L., Westler, W. M., and Markley, J. L. (2010) NMR investigations of the Rieske protein from *Thermus thermophilus* support a coupled proton and electron transfer mechanism. *J. Am. Chem. Soc.* **132,** 7908–7918
39. Saouma, C. T., Pinney, M. M., and Mayer, J. M. (2014) Electron transfer and proton-coupled electron transfer reactivity and self-exchange of synthetic [2Fe-2S] complexes: models for Rieske and mitoNEET clusters. *Inorg. Chem.* **53,** 3153–3161
40. Boron, W. F. (2004) Regulation of intracellular pH. *Adv. Physiol. Educ.* **28,** 160–179
41. Ciriolo, M. R., Palamara, A. T., Incerpi, S., Lafavia, E., Buè, M. C., De Vito, P., Garaci, E., and Rotilio, G. (1997) Loss of GSH, oxidative stress, and decrease of intracellular pH as sequential steps in viral infection. *J. Biol. Chem.* **272,** 2700–2708
42. Kalogeris, T., Baines, C. P., Krenz, M., and Korthuis, R. J. (2012) Cell biology of ischemia/reperfusion injury. *Int. Rev. Cell. Mol. Biol.* **298,** 229–317
43. Landry, A. P., Cheng, Z., and Ding, H. (2015) Reduction of mitochondrial protein mitoNEET [2Fe-2S] clusters by human glutathione reductase. *Free Radic. Biol. Med.* **81,** 119–127
44. Zhang, B., Crack, J. C., Subramanian, S., Green, J., Thomson, A. J., Le Brun, N. E., and Johnson, M. K. (2012) Reversible cycling between cysteine persulfide-ligated [2Fe-2S] and cysteine-ligated [4Fe-4S] clusters in the FNR regulatory protein. *Proc. Natl. Acad. Sci. U.S.A.* **109,** 15734–15739
45. Couturier, J., Touraine, B., Briat, J. F., Gaymard, F., and Rouhier, N. (2013) The iron-sulfur cluster assembly machineries in plants: current knowledge and open questions. *Front Plant Sci.* **4,** 259
46. Hall, J. W., Yang, J., Guo, H., and Ji, Y. (2015) The AirSR two-component system contributes to *Staphylococcus aureus* survival in human blood and transcriptionally regulates sspABC operon. *Front. Microbiol.* **6,** 682
47. Sun, F., Ji, Q., Jones, M. B., Deng, X., Liang, H., Frank, B., Telser, J., Peterson, S. N., Bae, T., and He, C. (2012) AirSR, a [2Fe-2S] cluster-containing two-component system, mediates global oxygen sensing and redox signaling in *Staphylococcus aureus*. *J. Am. Chem. Soc.* **134,** 305–314
48. Gaudu, P., and Weiss, B. (1996) SoxR, a [2Fe-2S] transcription factor, is active only in its oxidized form. *Proc. Natl. Acad. Sci. U.S.A.* **93,** 10094–10098
49. Kobayashi, K., Mizuno, M., Fujikawa, M., and Mizutani, Y. (2011) Protein conformational changes of the oxidative stress sensor, SoxR, upon redox changes of the [2Fe-2S] cluster probed with ultraviolet resonance Raman spectroscopy. *Biochemistry* **50,** 9468–9474
50. Ren, B., Duan, X., and Ding, H. (2009) Redox control of the DNA damage-inducible protein DinG helicase activity via its iron-sulfur cluster. *J. Biol. Chem.* **284,** 4829–4835
51. Boal, A. K., Yavin, E., and Barton, J. K. (2007) DNA repair glycosylases with a [4Fe-4S] cluster: a redox cofactor for DNA-mediated charge transport? *J. Inorg. Biochem.* **101,** 1913–1921
52. West, A. P., Shadel, G. S., and Ghosh, S. (2011) Mitochondria in innate immune responses. *Nat. Rev. Immunol.* **11,** 389–402
53. Giorgio, M., Migliaccio, E., Orsini, F., Paolucci, D., Moroni, M., Contursi, C., Pelliccia, G., Luzi, L., Minucci, S., Marcaccio, M., Pinton, P., Rizzuto, R., Bernardi, P., Paolucci, F., and Pelicci, P. G. (2005) Electron transfer between cytochrome c and p66Shc generates reactive oxygen species that trigger mitochondrial apoptosis. *Cell* **122,** 221–233
54. Finkel, T. (2012) Signal transduction by mitochondrial oxidants. *J. Biol. Chem.* **287,** 4434–4440
55. Marchi, S., Giorgi, C., Suski, J. M., Agnoletto, C., Bononi, A., Bonora, M., De Marchi, E., Missiroli, S., Patergnani, S., Poletti, F., Rimessi, A., Duszynski, J., Wieckowski, M. R., and Pinton, P. (2012) Mitochondria-ros crosstalk in the control of cell death and aging. *J. Signal Transduct.* **2012,** 329635
56. Galy, B., Ferring-Appel, D., Sauer, S. W., Kaden, S., Lyoumi, S., Puy, H., Kölker, S., Gröne, H. J., and Hentze, M. W. (2010) Iron regulatory proteins secure mitochondrial iron sufficiency and function. *Cell Metab.* **12,** 194–201
57. Styś, A., Galy, B., Starzyński, R. R., Smuda, E., Drapier, J. C., Lipiński, P., and Bouton, C. (2011) Iron regulatory protein 1 outcompetes iron regulatory protein 2 in regulating cellular iron homeostasis in response to nitric oxide. *J. Biol. Chem.* **286,** 22846–22854
58. Dixon, S. J., Lemberg, K. M., Lamprecht, M. R., Skouta, R., Zaitsev, E. M., Gleason, C. E., Patel, D. N., Bauer, A. J., Cantley, A. M., Yang, W. S., Morrison, B., 3rd, and Stockwell, B. R. (2012) Ferroptosis: an iron-dependent form of nonapoptotic cell death. *Cell* **149,** 1060–1072

Redox Control of the Human Iron-Sulfur Repair Protein MitoNEET Activity via Its Iron-Sulfur Cluster

Marie-Pierre Golinelli-Cohen, Ewen Lescop, Cécile Mons, Sergio Gonçalves, Martin Clémancey, Jérôme Santolini, Eric Guittet, Geneviève Blondin, Jean-Marc Latour and Cécile Bouton

J. Biol. Chem. 2016, 291:7583-7593.
doi: 10.1074/jbc.M115.711218 originally published online February 17, 2016